

## HOPF BIFURCATIONS IN CORONAL LOOPS I. STABILITY CONDITIONS FOR STATIC EQUILIBRIUM

D. GÓMEZ

Instituto de Astronomía y Física del Espacio, CONICET, Argentina

AND

A. SICARDI SCHIFINO AND C. FERRO FONTÁN

Facultad de Ciencias Exactas, Universidad de Buenos Aires, Argentina

Received 1988 August 29; accepted 1989 September 16

### ABSTRACT

We study the coupling between the hot plasma confined in a coronal loop and the much colder chromospheric plasma at the footpoints. Considering the coronal heating rate as a control parameter, we find that the static equilibrium becomes unstable for heating rates below a critical value, giving rise to the appearance of a stable limit cycle.

Starting from the hydrodynamic equations, we derive a model which generalizes the analysis of Kuin and Martens and consistently takes into account the condensation-evaporation process. In this paper, we linearize our equations in order to find the bifurcation point where the stability of the static equilibrium is lost. We also show that this model can provide a natural explanation for the excess widths of EUV spectral lines formed in the transition region. Moreover, we can predict the observed reduction in the broadening of these lines when they form in certain active regions, like quiescent prominences or sunspots.

*Subject headings:* hydromagnetics — Sun: corona

### I. INTRODUCTION

The high-resolution EUV and X-ray observations obtained by *Skylab* 15 years ago revealed a highly filamented corona composed by a wide variety of magnetic loop-like structures confining a very hot plasma ( $T \cong 10^6$  K).

Since these loops emit in soft X-rays during time scales much longer than their typical radiative cooling times, it seems adequate to describe them through a static energy balance between a heating source and conductive and radiative losses. Several static models which describe the thermal structure of coronal loops have been proposed (see Rosner, Tucker, and Vaiana 1978; also Craig, McClymont, and Underwood 1978; Vesecky, Antiochos, and Underwood 1979). From these equilibrium solutions, it is possible to derive *scaling laws* which satisfactorily describe the gross observed properties of the plasma confined in the loops under a wide range of conditions. However, these scaling laws do not reveal which is the true nature of the heating processes that contribute to heat the coronal plasma.

It is also important to notice that these equilibria must also be stable against small-amplitude perturbations if we expect to observe the system in these states. Fortunately, the stability analysis of a particular static equilibrium is much more informative with respect to the heating processes that take place than the equilibrium is itself, as has been shown by McClymont and Craig (1985*a, b*).

The linear theory of the thermal stability of static coronal loops has been investigated in a number of papers. Antiochos (1979) and Hood and Priest (1980) concluded that static loops are thermally unstable and thus the system must be in a ceaseless dynamic state. However, Chiuderi, Einaudi, and Torricelli-Ciamponi (1981) and also Craig and McClymont (1981) found that static equilibria are either stable or have a very small instability growth rate. The difference between both sets of papers lies in the treatment of the boundary conditions at the

base of the loop. For this reason, McClymont and Craig (1985*a*) and Antiochos *et al.* (1985) studied in detail the response of the chromospheric plasma to coronal perturbations in order to find appropriate boundary conditions for the coronal stability problem. Recent numerical studies of the nonlinear thermal evolution show that loops *taller* than  $5 \times 10^8$  cm are stable to finite amplitude perturbations (Klimchuk, Antiochos, and Mariska 1987).

However, the issue of nonlinear stability of coronal loops is an active field, where many questions still remain unanswered. For example, it is not clear which is the actual role of the chromospheric material in its interaction with the perturbed coronal plasma. A plausible stabilizing effect usually invoked in connection with solar flares is the so-called *evaporation-condensation* mechanism. Whenever a coronal temperature enhancement takes place, the corresponding increase of conductive flux to the bases drives an expansion of chromospheric material into the corona (evaporation). In this way, the coronal density and consequently the radiative losses grow up, thus contributing to stop the temperature enhancement. It seems reasonable to assume that this mechanism, as well as its reverse (condensation), also takes place (with lower intensity) in non-flaring regions. Moreover, Craig and McClymont (1987), using simple arguments, show that this must be the case for thermally stable loops. In this respect, Kuin and Martens (1982) produced a very interesting and comprehensive model, where the condensation-evaporation mechanism was phenomenologically considered. This simple model shows the global behavior of the corona when the coupling with the chromosphere is included and predicts that under certain conditions, a stable limit cycle appears in a density-temperature diagram. The major limitation of this model is that its equations are not a direct consequence of hydrodynamic considerations, as has been noticed by Craig and Schulkes (1985). However, the limit cycle behavior seems to be contained among the solutions of

the full set of hydrodynamic equations, as has been shown by Pakkert, Martens, and Verhulst (1987) using nonlinear diffusion asymptotic techniques.

A possible evidence of the existence of the evaporation-condensation process in nonflaring regions are the observed excess widths of EUV spectral lines formed in the transition region (see Cheng, Doschek, and Feldman 1976; Feldman and Doschek 1977). Typical *turbulence* velocities of roughly  $20 \text{ km s}^{-1}$  are inferred measuring the width of these lines. These velocities appear to be smaller over active regions like sunspots or quiescent prominences (Feldman and Doschek 1977), where values of about  $10 \text{ km s}^{-1}$  have been measured.

In this paper, we attempt to derive from the hydrodynamic equations a simple model which describes the main features of the coupling between the chromosphere and the corona. Moreover, we find that when the coronal heating rate falls below a certain critical value, the static equilibrium becomes unstable and the system evolves toward a limit cycle in the density-temperature diagram. In § II, we write down the general equations of the problem and describe briefly the set of equilibrium solutions (labeled by their heating rate value) whose linear stability we are going to study. In § III, the model equations are derived, and in § IV, we obtain the stability conditions for static equilibria as well as the critical heating rate value under which these equilibria are unstable. We also calculate the period of the limit cycle and the linear instability rate for the set of unstable solutions. The nonlinear saturation of this linear instability will be pursued both analytically and numerically in a future paper (Gómez, Sicardi Schifino, and Ferro Fontán 1990, hereafter Paper II). Finally, in § V, we discuss the results obtained and their observational implications. Upon estimating the typical velocity of material through the transition region, we show that our model can explain the excess width of spectral lines formed in this region. Assuming the dissipation of magnetic stresses driven by photospheric convection as a heating mechanism, we can show that the observed reduction of the Doppler width of these lines in magnetically active regions is due to the suppression of the limit cycle solution.

## II. GENERAL EQUATIONS AND EQUILIBRIUM SOLUTIONS

Due to the fact that the coronal magnetic field is strong enough, a one-dimensional hydrodynamic description of the plasma along each field line is well justified. Let us consider a coronal loop of half-length  $L$  along which we define a coordi-

nate  $z$  as shown in Figure 1. The hydrodynamic equations in this coordinate system are

$$\partial_t n = -\partial_z(nv), \quad (2.1a)$$

$$\partial_t(nv) = -\partial_z\left(\frac{P}{m_i} + nv^2\right) + ng, \quad (2.1b)$$

$$\frac{3}{2}\partial_t P = -\partial_z Q - \frac{5}{2}P\partial_z v + v\partial_z P - P^2\phi(T) + E, \quad (2.1c)$$

and the state equation between pressure ( $P$ ), particle density ( $n$ ), and temperature ( $T$ )

$$P = 2nk_B T, \quad (2.2)$$

holds, where  $k_B$  is the Boltzmann constant and  $m_i$  is the ion mass. The quantity  $v$  is the fluid velocity,  $g$  is the gravitational acceleration along the loop,  $Q$  is the classical heat flux

$$Q = -K_0 T^{5/2}\partial_z T, \quad (2.3)$$

$K_0 = 10^{-6} \text{ ergs K}^{-7/2} \text{ cm}^{-1} \text{ s}^{-1}$  is the thermal conductivity constant (Spitzer 1962),  $\phi(T)$  is the radiative loss function at constant pressure (see Martens and Kuin 1982), and  $E$  is the heating rate per unit volume. We have employed cgs units for all quantities except the temperature, which is expressed in K.

We have used the following radiative loss function (in the following,  $T_6$  is the temperature in MK):

$$\phi(T) = \begin{cases} 2.285 \times 10^{19}(T_6)^{9.7} & T_6 < 8.10^{-3}, \\ 1.313 \times 10^{14}(T_6) & 8.10^{-3} < T_6 < 10^{-1}, \\ 1.313 \times 10^{-3}(T_6)^{-3} & 10^{-1} < T_6, \end{cases} \quad (2.4)$$

where we have matched the fit of Peres *et al.* (1982) to an appropriate VAL model (Vernazza, Avrett, and Loeser 1981) for  $T < 8 \times 10^3 \text{ K}$ , to the fit of Craig and McClymont (1986). We also used

$$\phi(T) = \begin{cases} 2.295 \times 10^{19}(T_6)^{9.7} & T_6 < 8.10^{-3}, \\ 5.290 \times 10^7(T_6)^{4.15} & 8.10^{-3} < T_6 < 2.10^{-2}, \\ 2.209 \times 10^{-1}(T_6)^{-0.77} & 2.10^{-2} < T_6 < 10^{-1}, \\ 1.313 \times 10^{-9}(T_6)^{-3} & 10^{-1} < T_6, \end{cases} \quad (2.5)$$

in order to test the influence of the Ly $\alpha$  losses in our calculations.

We will consider both the coronal and chromospheric parts of the loop with sizes much smaller than their corresponding

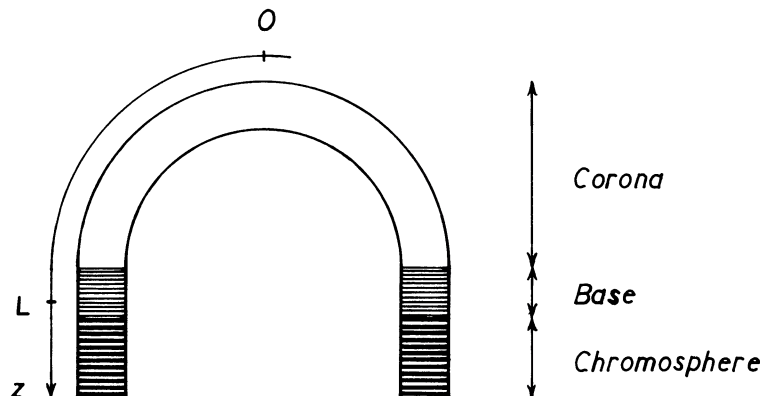


FIG. 1.—Schematic view of a coronal loop

height scales ( $H = 2k_B T/m_i g$ ). Thus, we neglect gravity effects, and as a consequence, the pressure equilibrium simply reads  $P = \text{const}$  throughout the loop. The static equilibrium equations corresponding to equations (2.1)–(2.3) are

$$v = 0 = \partial_z P_0, \quad (2.6)$$

$$\partial_z Q = E - P_0^2 \phi(T_0), \quad (2.7a)$$

$$Q = -K_0 T_0^{5/2} \partial_z T_0, \quad (2.7b)$$

where  $\phi(T)$  is the function detailed in equation (2.4). Because of the symmetry of the loops, we consider  $Q(z=0) = 0$ . The other boundary condition needed to solve equation (2.7) will be  $Q(z=L) = 0$ . This type of equilibria is usually called the *isolated loop*, and it has been shown (see Antiochos 1979) that they are unstable if the same boundary conditions are also applied to the perturbation field. We extend this coronal equilibrium into the chromosphere at the constant temperature  $T_{0b}$  which satisfies

$$E_b = P_0^2 \phi(T_{0b}), \quad (2.8a)$$

$$E_b = \frac{E}{1 - \gamma^*} \quad 0 \leq \gamma^* < 1. \quad (2.8b)$$

This equilibrium includes corona, transition region, and upper chromosphere and assumes a spatial discontinuity in the heating rate. For any positive value of  $\gamma^*$ , the temperature  $T_{0b}$  is reached at a finite distance below the transition region. But as  $\gamma^*$  goes to zero (spatially continuous heating rate), this distance becomes infinite. This fact has been carefully discussed by Craig, Robb, and Rollo (1982), and more recently by McClymont and Craig (1985a), who define a parameter  $\gamma^*$  in a way equivalent to equation (2.8b).

The above considerations define a family of equilibria with three free parameters ( $E$ ,  $L$ , and  $\gamma^*$ ). For this reason, we shall hereafter take  $E$  and  $\gamma^*$  as the control parameters for a given loop of half-length  $L$ . According to our model, once the values of  $E$  and  $\gamma^*$  are fixed, the static equilibrium and its stability can be univocally derived.

Following usual procedures (see Withbroe 1981; also Rosner, Tucker, and Vaiana 1978), we obtain scaling laws quite

comparable to those obtained by Rosner, Tucker, and Vaiana (1978) or Craig, McClymont, and Underwood (1978). Our scaling laws (see Fig. 2) are

$$P_0 L = C_p (EL^2)^{\beta_p} = 0.029 \text{ ergs cm}^{-3} (EL^2)^{0.911}, \quad (2.9a)$$

$$T_0 = C_T (EL^2)^{\beta_T} = 0.575 \times 10^6 \text{ K} (EL^2)^{0.286}, \quad (2.9b)$$

$$T_{0b} = C_b (EL^2)^{\beta_b} = 8.21 \times 10^3 \text{ K} (EL^2)^{-0.085}, \quad (2.9c)$$

where  $E$  is expressed in  $(1/9000) \text{ ergs cm}^{-3} \text{ s}^{-1}$  units and  $L$  is expressed in  $3 \times 10^9 \text{ cm}$  units. We have checked that the excess of radiative losses through  $\text{Ly}\alpha$  does not appreciably affect our equilibria (the relative departure remains below 5%). We have also checked that even when the temperature profile becomes very steep in the transition region, the conductive flux never exceeds 1% of the saturated flux value corresponding to that temperature [ $Q_{\text{sat}} = \frac{1}{4} n m_e (k_B T/m_e)^{3/2}$ , where  $m_e$  is electron mass]. This result is in coincidence with a similar conclusion of Somov (1978) in connection with solar flares and shows that the Spitzer's formula for conductivity remains applicable.

### III. DERIVATION OF THE MODEL EQUATIONS

Following Kuin and Martens (1982), we recognize three different time scales associated with the problem. A dynamical time scale

$$\tau_d = \Delta z / c_s \quad (3.1)$$

(where  $c_s$  is the speed of sound and  $\Delta z$  is a typical length), during which pressure inhomogeneities relax, a radiative time scale

$$\tau_r = \frac{3}{2P\phi(T)}, \quad (3.2)$$

during which thermal equilibrium is achieved through radiative losses, and a conductive time scale

$$\tau_c = \frac{3P(\Delta z)^2}{2K_0 T^{7/2}}, \quad (3.3)$$

during which thermal inhomogeneities smooth out. For coronal conditions  $\tau_d^{\text{cor}} \ll \tau_c^{\text{cor}} \ll \tau_r^{\text{cor}}$ , while in the chromo-

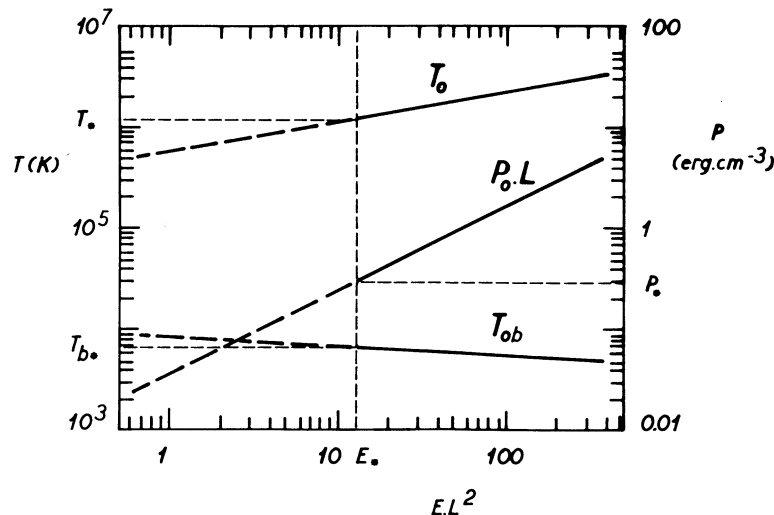


FIG. 2.—Scaling laws derived from our static equilibrium model. The quantities  $T_0$ ,  $T_{0b}$ , and  $P_0 L$  are plotted as functions of  $EL^2$ . Dashed line indicates unstable static equilibria (for  $\gamma^* = 0.05$ ).

sphere, these relations are significantly altered, being  $\tau_d^{\text{chr}} \ll \tau_c^{\text{chr}} \ll \tau_d^{\text{cor}}$  and  $\tau_d^{\text{chr}} \leq \tau_d^{\text{cor}}$ . Therefore, if we are interested in the evolution of the system at the time scale  $\tau_c^{\text{cor}}$ , we can suppose pressure equilibrium ( $\tau_d \ll \tau_c^{\text{cor}}$ ) and also thermal equilibrium in the chromosphere ( $\tau_r^{\text{chr}} \ll \tau_c^{\text{cor}}$ ). Due to its fast relaxation, the chromospheric thermal balance immediately adapts to the coronal changes.

Because of the above considerations, we believe that a very simplified model which retains some of the relevant features of the true problem, can be a spatially uniform corona (which includes the transition region) in contact with another spatially uniform thin region of the upper chromosphere which we call the *base*. We define the base as a thin region of the upper chromosphere (centered around  $z = L$ ) which is reactive to thermal perturbations of the coronal plasma (see Fig. 3). We are going to consistently find the temporal evolution of the hydrodynamic quantities describing the material contained in the base and the one contained in the corona. For this purpose, we perform spatial averages of the exact hydrodynamic equations and model the fluxes between these regions. We consider density, temperature, and pressure to be of the form

$$f(z, t) = f_0(z)[1 + \delta f(t)], \quad (3.4a)$$

$$f_b(z, t) = f_{0b}(z)[1 + \delta f_b(t)], \quad (3.4b)$$

where  $f_0(z)$  is the static equilibrium (see § II) and  $\delta f(t)$  is the nonlinear separation from the equilibrium value. The subscript “b” indicates the part of the function corresponding to the base. Carrying over this form into equations (2.1) and spatially averaging throughout the corona (plus transition region)

$$n_0 \partial_t \delta n = -\frac{1}{L} (1 + \delta n_b) n_{0b} v_b^-, \quad (3.5a)$$

$$0 = \partial_z P_0, \quad (3.5b)$$

$$\frac{3}{2} P_0 \partial_t \delta p = -\frac{Q_L}{L} - \frac{5}{2} P_0 (1 + \delta p) \frac{v_b^-}{L} + E[1 - (1 + \delta p)^2 (1 + \delta T)^\gamma], \quad (3.5c)$$

where  $Q_L$  is the heat flux reaching the base and  $v_b^-$  is the fluid

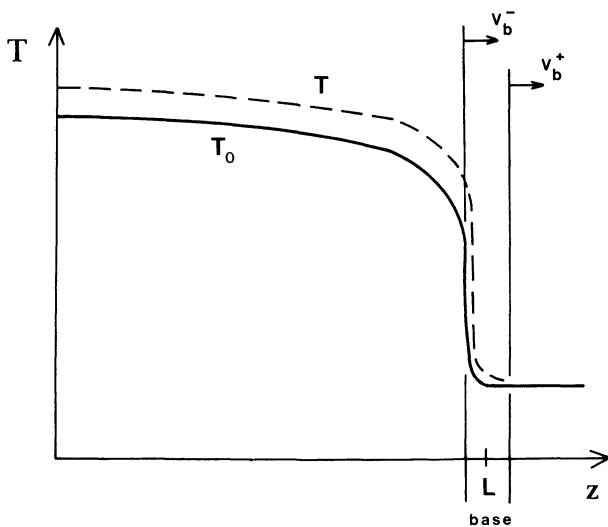


FIG. 3.—Static thermal distribution along the  $z$ -axis [ $T_0(z)$ ], indicating the location of the base. Dashed line corresponds to the time-dependent temperature distribution  $T(z, t) = T_0(z)[1 + \delta T(t)]$  assumed in our model.

velocity through the base-corona interface. Similarly, we will call  $v_b^+$  the fluid velocity crossing the bottom of the base. The exponent  $\gamma$  is the power of the function  $\phi(T)$  at coronal temperatures ( $\gamma = -3$ ; see eq. [2.4]). We have employed the notation

$$f_0 = \int_0^L \frac{dz}{L} f_0(z). \quad (3.6)$$

Since the equilibria we consider are those whose conductive fluxes vanish at the bases of the loop (see § II),  $Q_L$  will be nonzero only when perturbations are present. Because we place the point  $z = L$  just below the transition region of these equilibria, we propose  $Q_L$  to be

$$Q_L = \frac{1}{L_b} K_0 T_{0b}^{5/2} T_0 \delta T, \quad (3.7)$$

where  $L_b$  is the base thickness. If we develop our equilibrium solution  $T_0(z)$  linearly around  $z = L$ , we find (see Appendix) using equations (2.7) and (2.8) that in the very low transition region, the temperature exponentially approaches the value  $T_{0b}$  on a typical length scale which we identify as  $L_b$ ,

$$L_b = \left( \frac{K_0 T_{0b}^{7/2}}{\gamma_b E} \right)^{1/2} \ln \left( 2 + \frac{2\gamma_b (e-1)}{\gamma^*} \right). \quad (3.8)$$

Notice that (as has been remarked in § II) the singularity for  $\gamma^* \rightarrow 0$  implies here that  $L_b$  goes logarithmically to infinity as predicted by Craig, Robb, and Rollo (1982). Of course, this result does not imply that the whole chromosphere reacts to coronal perturbations, but simply that equation (3.8) is not valid to define  $L_b$ . For this reason, we are not going to consider the  $\gamma^* \rightarrow 0$  case in our model.

Because of the very large conductive time scale of the chromosphere, we are going to consider the base as energetically decoupled from the rest of the chromosphere. However, due to the very short dynamic time scale, we suppose that the chromosphere instantaneously replenishes or evacuates the base according to the requirements of the condensation-evaporation process. Thus, the base is maintained at constant density throughout its evolution ( $\delta n_b = 0$ ). This condition is actually satisfied whether the fluid crosses this region in a time shorter than the time scale in which we are interested ( $\tau_c^{\text{cor}}$ ). Whenever coronal loops evolve exhibiting limit cycle behavior, we expect  $v \approx L/\tau_c^{\text{cor}}$ . Thus, the crossing time throughout the base results in  $(L_b/v) \approx (L_b/L)\tau_c^{\text{cor}} \ll \tau_c^{\text{cor}}$ , as asserted above. Since both this typical time scale for mass flow and the thermal relaxation time are much shorter than  $\tau_c^{\text{cor}}$ , the base instantaneously achieves a stationary state, its evolution is therefore *enslaved* to the coronal perturbations.

Computing the spatial average of equations (2.1a) and (2.1c) in the base, we find

$$n_{0b}^- v_b^- = n_{0b}^+ v_b^+, \quad (3.9a)$$

$$0 = \frac{Q_L}{L_b} + \frac{5}{2} P_0 (1 + \delta p) \frac{1}{L_b} (v_b^- - v_b^+) + E_b [1 - (1 + \delta p)^2 (1 + \delta T_b)^\gamma]. \quad (3.9b)$$

According to the definition of  $L_b$  (see Appendix), we find

$$v_b^+ \cong \frac{1}{e} v_b^-. \quad (3.10)$$

We can use this relation in equation (3.9) to obtain an expression for  $v_b^-$  as a function of the perturbations,

$$v_b^- = -\frac{2}{5} \frac{e}{e-1} \times \left[ \frac{K_0 T_{0b}^{5/2} T_0}{P_0 L_b} \frac{\delta T}{1+\delta p} + \frac{E_b L_b}{P_0} \frac{1-(1+\delta p)^{\gamma_b+2}}{1+\delta p} \right]. \quad (3.11)$$

The temperature perturbations are calculated with the aid of the state equation (2.2):

$$\delta T = (\delta p - \delta n)/(1 + \delta n), \quad (3.12a)$$

$$\delta T_b = \delta p. \quad (3.12b)$$

Substituting equations (3.7) through (3.12) into equation (3.5), we obtain

$$\partial_\tau \delta n = \frac{1}{1+\delta p} \left\{ \alpha \delta T + \beta \frac{h}{\theta} \left[ 1 - (1+\delta p)^{\gamma_b+2} \right] \right\}, \quad (3.13a)$$

$$\partial_\tau \delta p = 1 - (1+\delta p)^2 (1+\delta T)^\gamma + \frac{5}{3} \beta h [1 - (1+\delta p)^{\gamma_b+2}] + \frac{5}{3e} \alpha \theta \delta T, \quad (3.13b)$$

where

$$\alpha = \frac{3}{5} \frac{e}{e-1} \frac{K_0 T_{0b}^{3/2} T_0^2}{EL^2 h}, \quad \beta = \frac{3}{5} \frac{e}{e-1} \frac{1}{1-\gamma^*}, \quad (3.13c)$$

and  $\tau = (2E/3P_0)t$  is roughly the time in  $\tau_r^{\text{cor}}$  units,  $h = L_b/L$  and  $\theta = T_{0b}/T_0$  are dimensionless functions of  $E$  (of order  $\ll 1$ ). Relations (3.12) and (3.13) constitute the full set of equations which describe the nonlinear evolution of our simplified chromosphere-corona model.

#### IV. ANALYSIS OF LINEAR STABILITY

Linearizing equation (3.13) with respect to the perturbations  $\delta n$  and  $\delta p$ , we find

$$\partial_\tau \psi = \mathbf{L} \cdot \psi \quad (4.1)$$

where

$$\psi = \begin{pmatrix} \delta n \\ \delta p \end{pmatrix}, \quad (4.2)$$

and

$$\mathbf{L} = \begin{pmatrix} -\alpha & \alpha - \beta \frac{h}{\theta} (\gamma_b + 2) \\ \gamma - \frac{5}{3e} \alpha \theta & -\gamma - 2 - \frac{5}{3} \beta h (\gamma_b + 2) + \frac{5}{3e} \alpha \theta \end{pmatrix}. \quad (4.3)$$

As is well known, the stability or instability of the equilibria under consideration is connected with the sign of the real part of the eigenvalues of the matrix  $\mathbf{L}$ :

$$\lambda_{1,2} = \frac{L_{11} + L_{22}}{2} \pm \sqrt{\frac{(L_{11} + L_{22})^2}{4} - (L_{11} L_{22} - L_{12} L_{21})}. \quad (4.4)$$

We calculated these eigenvalues for  $E$  varying within the range  $10^{-1}$  to  $10^{-5}$  ergs  $\text{cm}^{-3} \text{s}^{-1}$  and  $\gamma^*$  between 0 and 0.5 and found that they always satisfy  $\lambda_2^* = \lambda_1$ . As predicted by elementary stability theory (see, for instance, Iooss and Joseph 1980),

a Hopf bifurcation takes place whenever the real part of a pair of complex conjugate eigenvalues changes from a negative to a positive sign. An examination of expression (4.4) immediately reveals that a Hopf bifurcation appears when the trace of  $\mathbf{L}$  crosses the zero while the determinant remains positive. We find from equation (4.3) and by applying the scaling laws in equation (2.9) the region in the plane of parameters  $(\gamma^*, EL^2)$  where the static equilibrium is linearly unstable. This region has been shaded in Figure 4a, where we see that for any given small value of  $\gamma^*$ , there exists a critical value,  $(EL^2)_*$ , below which the static equilibrium is not stable, and a limit cycle solution takes place. For situations close to the critical ( $E = E_*$ ), the period of the limit cycle is given by the expression

$$\tau_0 = 2\pi \frac{3P_0}{2E} \det^{-1/2}(\mathbf{L}). \quad (4.4)$$

Figure 4b shows the dependence of this period upon the parameter  $\gamma^*$ . For any choice of parameters inside the shaded region of Figure 4a, the system is attracted to a stable limit cycle, as is schematically shown in Figure 5. The amplitude of this cycle as a function of the heating rate as well as its stability will be described in Paper II both analytically and numerically.

Hereafter and just as an illustrative example, we are going to consider

$$\gamma^* = 0.05, \quad (4.5)$$

and we reserve the subscript “\*” to refer to a quantity evaluated at the critical point. We obtained

$$(EL^2)_* = 12.5, \quad (4.6a)$$

$$T_* = 1.2 \times 10^6 \text{ K}, \quad (4.6b)$$

$$T_{b*} = 6.6 \times 10^3 \text{ K}, \quad (4.6c)$$

$$P_* L = 0.3 \text{ ergs cm}^{-3}, \quad (4.6d)$$

$$L_{b*} = 2.5 \text{ km}. \quad (4.6e)$$

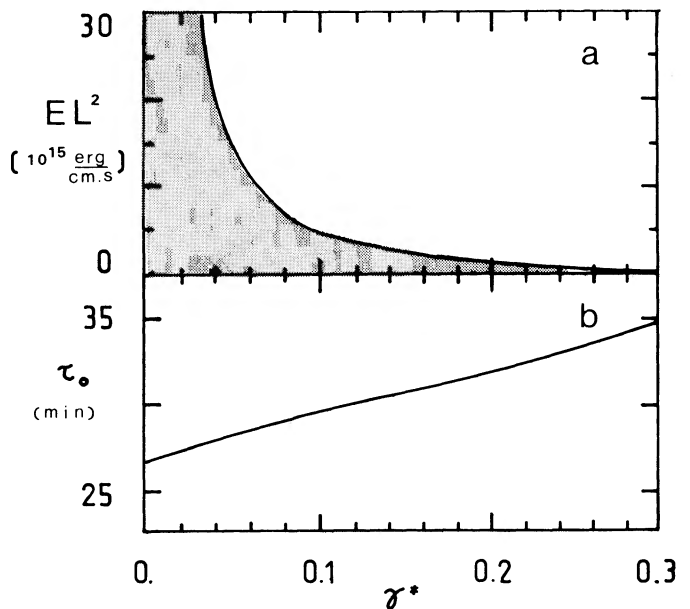


FIG. 4.—(a) Critical value of the parameter  $EL^2$  (in units of  $10^{15}$  ergs  $\text{cm}^{-3} \text{s}^{-1}$ ) as a function of  $\gamma^*$ . Shaded region corresponds to linearly unstable static equilibria. (b) Period of the limit cycle (evaluated at the critical point) as a function of  $\gamma^*$ .

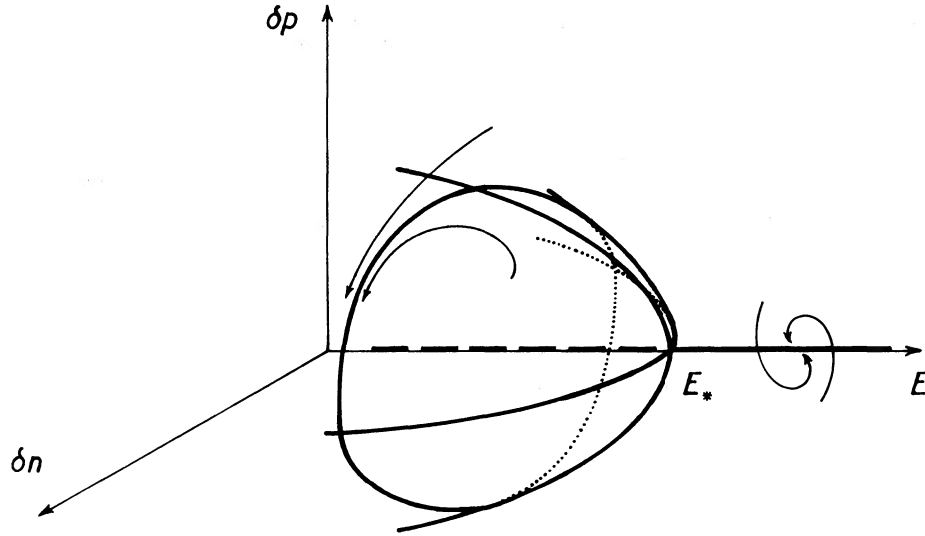


FIG. 5.—Schematic diagram showing the static and limit cycle equilibria. Dashed line indicates unstable equilibria.

From equation (3.11), we can derive the order of magnitude of the velocity fields that cross along the bases of the loop. Evaluating equation (3.11) close to the critical point, we get a lower limit for  $v_b^-$ , since it is a decreasing function of  $EL^2$ . Keeping terms up to the first order in  $\delta n$  and  $\delta p$ , we find that the second term in equation (3.11) becomes negligible compared to the first, thus resulting in

$$v_{b*}^- = -0.54 \text{ km s}^{-1} \delta p. \quad (4.7)$$

As we have shown in § III, the mass flow through the base can be regarded as stationary (with  $nv$  spatially constant). Given that pressure is constant along the loop, we find that velocity increases linearly with temperature. Therefore, if we imagine a loop as a bundle of thermally independent flux tubes, each undergoing a limit cycle but with phases evenly distributed, we can estimate the Doppler width of a line forming in a region of temperature around  $T$  as

$$\Delta\nu(T) = 1.08 \text{ km s}^{-1} \frac{T}{T_b} \delta p_{\max}, \quad (4.8)$$

where a factor of 2 has been applied to equation (4.7) to account for the upside and downside flow directions, and where  $\delta p_{\max}$  is the amplitude of  $\delta p(t)$ .

#### V. DISCUSSION

We note the relatively low value of our base temperature (see eq. [4.6c]), which is about a factor of 1.5 below its typical range. This fact reflects the fictitious equilibrium model that we have used to match the coronal isolated loop solution with the chromospheric one in a simple expression. This kind of oversimplification when modeling the chromosphere-corona interface has been widely applied (Peres *et al.* 1982; An *et al.* 1983; Klimchuk, Antiochos, and Mariska 1987) and shown a lack of detailed knowledge of the true behavior of this thin region of the solar atmosphere. The chromospheric heating mechanism as well as its radiative behavior still remains unclear (McClymont and Canfield 1983; Athay 1986). Moreover, Shoub (1983) has shown that kinetic effects are likely to be relevant in this region. Further investigation of this subject is

obviously quite important, but due to its complexity, we have considered it beyond the scope of the present work.

Since we are able to consistently follow the temporal evolution of both the base and the corona, we can derive an estimate of the coupling factor  $f$  defined by Kuin and Martens (1982). We write down their evolution equations in the notation employed throughout this work:

$$\partial_\tau \delta n = f \alpha_{\text{KM}} \frac{\delta T}{1 + \delta T}, \quad (5.1a)$$

$$\partial_\tau \delta p = 1 - (1 + \delta p)^2 (1 + \delta T)^\gamma, \quad (5.1b)$$

where

$$\alpha_{\text{KM}} = \frac{K_0 T_0^{7/2}}{EL^2}, \quad (5.2)$$

and the factor  $f$  ( $0 \leq f \leq 1$ ) is the fraction of downward conductive flux which is effective in evaporating chromospheric material. We find two main differences with respect to our equations (3.13). The first is that equation (5.1) looks like the asymptotic limit  $h = 0$  and  $\theta \rightarrow 0$  of equation (3.13). This is an expected result, since Kuin and Martens do not include chromospheric plasma in their model. The second difference arises because of the different location of the chromosphere-corona interface ( $z = L$ ) in both models. This fact is reflected in the different expressions of the  $\alpha$  coefficients and also in the denominator  $(1 + \delta T)$  in equation (5.1a), which according to our model, should be  $(1 + \delta T_b)$  (see eqs. [3.12b] and [3.13a]). Matching both coefficients

$$\alpha = f \alpha_{\text{KM}}, \quad (5.3)$$

we obtain, evaluating at the critical point,

$$f_* = \frac{3}{5} \frac{e}{e-1} \frac{\theta_*^{3/2}}{h_*} \cong 4.6, \quad (5.4)$$

which is a number larger than 1, in contradiction with the definition of Kuin and Martens (1982). We agree with Craig and Schulkes (1985) in the fact that there is no need for  $f$  to be

defined within the range  $[0, 1]$ , since it is theoretically possible for the corona to extract more energy as enthalpy from the chromosphere than the energy delivered as excess conductive flux. We note also that according to expression (5.2) and to the scaling laws, the  $\alpha_{KM}$  coefficient is independent of the heating rate, and thus the coronal heating does not control the stability or instability as it does in our model.

We now consider some possible observational consequences of the limit cycle behavior. As has been stated in the previous section (see also Kuin and Martens 1982), due to the extremely low conductivity transverse to the magnetic field, a coronal loop can be considered as a set of magnetic plasma columns, each undergoing a cyclic thermal evolution with a unique period but with their phases randomly distributed. Thus, in this case, a coronal loop should not be considered as a thermal structure but as a superposition of thermal structures whose mean temperature corresponds to the one predicted by the scaling laws. For this reason, observations taken with low-resolution soft X-ray detectors may not distinguish between static and limit cycle equilibria. But the fluid velocities involved in the cyclic evaporation-condensation mechanism should produce observable Doppler shifts of spectral lines. The nonthermal broadening of spectral lines formed in the lower transition region has been observed and studied by several authors (Cheng, Doschek, and Feldman 1976; Feldman and Doschek 1977, and references therein). We suggest that the limit cycle behavior can naturally explain this broadening. To show this, we have derived an estimate for the fluid velocity  $v_b^-$  at the base-corona interface (eq. [4.7]). The superposition of those phase-unrelated Doppler shifts should result in a broadening of the line whose width becomes univocally related to the amplitude of the limit cycle and consequently to the heating rate (see eq. [4.8]). In Figure 6, we compare the velocity-temperature correlation found by Cheng, Doschek, and Feldman (1976), measuring Doppler widths of lines formed at different depths with our theoretical relation (4.8) evaluated at different values of the control parameter  $E/E_*$ . The detailed calculation of the amplitude of the cycle ( $\delta p_{\max}$ ) as a function of the parameter  $EL^2$  used to compute  $\Delta v(T)$  in equation (4.8) is shown in Paper II. The approximately linear relationship shown by the observational results in Figure 6 supports our hypothesis of steady mass flow through the base ( $\delta n_b = 0$ ).

It is important to note that the existence of limit cycles provides a unified description of both a dynamic transition region (evidenced by anomalous Doppler widening) and a globally static corona (as results from soft X-ray observations and their comparison with scaling laws). Moreover, for sufficiently low amplitude limit cycles (such as those under consideration here), this dynamic attractor could hardly be distinguished from the static solution in time-dependent numerical computations (like Craig, Robb, and Rollo 1982).

Craig and McClymont (1987) also derive a set of ordinary differential equations that describe the global behavior of the corona. They conclude that the interaction with the upper chromosphere is essential for stabilizing the thermal evolution of coronal loops. However, because they place the  $z = L$  level far below the conductively influenced region, they do not obtain limit cycle behavior, because it has been swept in their spatial average.

Another interesting result we want to discuss is the expression (4.6a) for the critical heating rate value which depends on  $L$  as  $L^{-2}$ . If the heating mechanism invoked is Joule dissi-

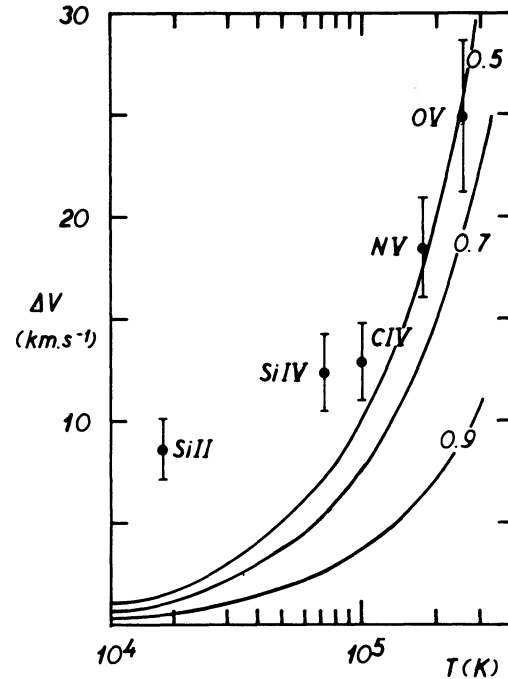


FIG. 6.—Dots with their corresponding error bars are from Cheng, Doschek, and Feldman (1976). The full line is our theoretical best fit and corresponds to  $EL^2 = 0.6(EL^2)_*$  (see Paper II).

pation of magnetic stresses excited by photospheric convection (cf. Parker 1981*a, b*; 1983*a, b*; see also Sturrock and Uchida 1981; Gómez and Ferro Fontán 1988), the heating rate is

$$E = \frac{u_p^2 \tau_p B_0^2}{4\pi L^2}, \quad (5.5)$$

where  $u_p$  and  $\tau_p$  are the typical velocity and turnover time of the photospheric eddies associated with granulation, while  $B_0$  is the magnetic field along the loop. Thus, looking at relations (4.6a) and (5.5), we see that the stability or instability of the system does not depend on the length of the loop but on the intensity of photospheric convection and magnetic field of the loop,

$$u_{p5}^2 \tau_{p3} B_z^2 < 1.5, \quad (5.6)$$

where  $u_{p5}$  is the photospheric velocity field in  $10^5$  cm,  $\tau_{p3}$  is the eddy turnover time in  $10^3$  s, and  $B_z$  is the magnetic field in  $10^2$  G. Under the hypothesis of approximately constant photospheric activity throughout the solar surface, the above result implies that limit cycles should preferably exist in loops of arbitrary length, but with a relatively low magnetic field. This theoretical conclusion appears to be in close agreement with the reduced nonthermal broadening reported by Feldman and Doschek (1977) of about  $10 \text{ km s}^{-1}$  in quiescent prominences and sunspots. But the excess widths of lines formed in these magnetically active regions, however small, remains unexplained. Because of the uncertainties involved in our estimates, we cannot rule out the existence of other broadening mechanisms. Since the relaxation time to equilibrium becomes too large near the bifurcation point ( $\text{Re}[\lambda] \rightarrow 0$  in eq. [4.4]), we speculate that the ensemble of transients caused by random perturbations can give an extra broadening of the lines on both sides of the bifurcation point, that is, on both quiet-sun and active regions.

The detailed calculation of the amplitude of the limit cycle, as well as the relaxation time of this dynamical equilibrium state, will be developed in Paper II, both analytically (following a perturbative method valid in the neighborhood of the critical point) and numerically (solving the eq. [3.13] for arbitrary values of  $E$ ).

We gratefully acknowledge M. Machado for very useful comments and suggestions. This work was supported by the Consejo Nacional de Investigaciones Científicas y Técnicas (CONICET, Argentina) under Grant 9069/03, and one of us (D. G.) has been honored with a fellowship of this institution.

## APPENDIX

### ESTIMATE OF THE BASE THICKNESS

We express the equilibrium temperature near the base ( $z \cong L$ ) as

$$T(z) = T_{0b}[1 + f(z)], \quad (\text{A1})$$

where  $f(z)$  must satisfy the equilibrium equation

$$\gamma_b \partial_\xi [(1 + f)^{5/2} \partial_\xi f] = \frac{(1 + f)^{\gamma_b}}{1 - \gamma^*} - 1, \quad \xi = (L - z) \sqrt{\frac{\gamma_b E}{K_0 T_{0b}^{7/2}}}, \quad (\text{A2})$$

and the boundary conditions

$$f(0) = 0 = \partial_\xi f(0). \quad (\text{A3})$$

The only solution of equation (A2) under conditions (A3) for  $\gamma^* = 0$  is  $f(\xi) = 0$ . For  $0 < \gamma^* \ll 1$ , we can assume  $f = \gamma^* f_1 + (\gamma^*)^2 f_2 + \dots$ , and keeping terms up to the first order in  $\gamma^*$ , we find

$$\partial_{\xi\xi} f_1 - f_1 = \gamma_b^{-1}, \quad (\text{A4})$$

thus

$$f_1 = \gamma_b^{-1} (\cosh \xi - 1). \quad (\text{A5})$$

This solution increases approximately exponentially with  $\xi$ . We define the  $e$ -rising length scale  $\xi_b$  as

$$1 + f(\xi_b) = e = 2.718\dots, \quad (\text{A6})$$

and thus we find from equation (A5)

$$\xi_b \cong \ln \left[ 2 + \frac{2\gamma_b(e-1)}{\gamma^*} \right]. \quad (\text{A7})$$

According to the relationship (A2) between the variables  $z$  and  $\xi$ , we can derive the following expression for the base thickness:

$$L_b = \left( \frac{K_0 T_{0b}^{7/2}}{\gamma_b E} \right)^{1/2} \xi_b. \quad (\text{A8})$$

## REFERENCES

- An, C. H., Canfield, R., Fisher, G. H., and McClymont, A. N. 1983, *Ap. J.*, **267**, 421.  
 Antiochos, S. K., 1979 *Ap. J. (Letters)*, **232**, L125.  
 Antiochos, S. K., Shoub, E. C., An, C. H., and Emslie, A. G. 1985, *Ap. J.*, **298**, 876.  
 Athay, R. G. 1986, *Ap. J.*, **308**, 975.  
 Cheng, C., Doschek, G. A., and Feldman, U. 1976, *Ap. J.*, **210**, 836.  
 Chiuderi, C., Einaudi, G., and Torricelli-Ciamponi, G. 1981, *Astr. Ap.*, **97**, 27.  
 Craig, I. J. D., and McClymont, A. N. 1981, *Nature*, **294**, 333.  
 ———. 1986, *Ap. J.*, **307**, 367.  
 ———. 1987, *Ap. J.*, **318**, 421.  
 Craig, I. J. D., McClymont, A. N., and Underwood, J. H. 1978, *Astr. Ap.*, **70**, 1.  
 Craig, I. J. D., Robb, T. D., and Rollo, M. D. 1982, *Solar Phys.*, **76**, 331.  
 Craig, I. J. D., and Schulkes, R. M. S. M. 1985, *Ap. J.*, **296**, 710.  
 Feldman, U., and Doschek, G. A. 1977, *Ap. J. (Letters)*, **216**, L119.  
 Gómez, D., and Ferro Fontán, C. 1988, *Solar Phys.*, **116**, 33.  
 Gómez, D., Sicardi Schifino, A., and Ferro Fontán, C. 1990, *Ap. J.*, **352**, 326.  
 Hood, A. W., and Priest, E. R. 1980, *Astr. Ap.*, **87**, 126.  
 Iooss, G., and Joseph, D. D. 1980, *Elementary Stability and Bifurcation Theory* (Berlin: Springer-Verlag).  
 Klimchuk, J. A., Antiochos, S. K., and Mariska, J. T. 1987, *Ap. J.*, **320**, 409.  
 Kuin, N. P. M., and Martens, P. C. H. 1982, *Astr. Ap.*, **106**, L1.  
 Martens, P. C. H., and Kuin, N. P. M. 1982, *Astr. Ap.*, **112**, 366.  
 McClymont, A. N., and Canfield, R. C. 1983, *Ap. J.*, **265**, 497.  
 McClymont, A. N., and Craig, I. J. D. 1985a, *Ap. J.*, **289**, 820.  
 ———. 1985b, *Ap. J.*, **289**, 843.  
 Pakkert, J. W., Martens, P. C. H., and Verhulst, F. 1987, *Astr. Ap.*, **179**, 285.  
 Parker, E. N. 1981a, *Ap. J.*, **244**, 631.  
 ———. 1981b, *Ap. J.*, **244**, 644.  
 ———. 1983a, *Ap. J.*, **264**, 635.  
 ———. 1983b, *Ap. J.*, **264**, 642.  
 Peres, G., Rosner, R., Serio, S., and Vaiana, G. S. 1982, *Ap. J.*, **252**, 791.  
 Rosner, R., Tucker, W. H., and Vaiana, G. S. 1978, *Ap. J.*, **220**, 643.  
 Shoub, E. C., 1983, *Ap. J.*, **266**, 339.  
 Somov, B. V. 1978, *Solar Phys.*, **60**, 315.  
 Spitzer, L. 1962, *Physics of Fully Ionized Gases* (New York: Interscience).  
 Sturrock, P. A., and Uchida, Y. 1981, *Ap. J.*, **246**, 331.  
 Vernazza, J. E., Avrett, E. H., and Loeser, R. 1981, *Ap. J. Suppl.*, **45**, 635.  
 Vesceky, J. F., Antiochos, S. K., and Underwood, J. H. 1979, *Ap. J.*, **233**, 987.  
 Withbroe, G. L. 1981, in *Solar Active Regions*, ed. F. Q. Orrall (Boulder, CO: Colorado Associated University Press), p. 199.

CONSTANTINO FERRO FONTÁN and ANIBAL SICARDI SCHIFINO: Departamento de Física, Facultad de Ciencias Exactas y Naturales—Universidad de Buenos Aires, Ciudad Universitaria (1428) Buenos Aires, Argentina

DANIEL GÓMEZ: Instituto de Astronomía y Física del Espacio, C.C. 67 - Suc. 28, (1428) Buenos Aires, Argentina

## HOPF BIFURCATIONS IN CORONAL LOOPS. II. NONLINEAR EVOLUTION OF INSTABILITIES

D. GÓMEZ

Instituto de Astronomía y Física del Espacio, CONICET, Argentina

AND

A. SICARDI SCHIFINO AND C. FERRO FONTÁN

Facultad de Ciencias Exactas, Universidad de Buenos Aires, Argentina

Received 1988 September 22; accepted 1989 September 16

### ABSTRACT

In a previous paper, we have modeled the coupling between corona and chromosphere and derived a nonlinear set of equations, where the global stability properties of the coronal plasma can be studied. The linear stability analysis indicates that the static equilibrium is stable unless the heating rate falls below a certain critical value.

In the present paper, we study the nonlinear evolution of our equations both analytically and numerically. Applying a perturbative technique around the critical point, we find that a subcritical Hopf bifurcation takes place. The numerical integration of the equations agrees satisfactorily with the analytical results when they are compared close to the bifurcation. The nonthermal Doppler widths of EUV lines forming in the transition region can be explained by the existence of relatively low amplitude limit cycles.

*Subject headings:* hydromagnetics — Sun: chromosphere — Sun: corona

### I. INTRODUCTION

Since the hot plasma confined in coronal loops is observed emitting in soft X-rays during time scales much longer than their typical radiative cooling time, it seems clear that a stable thermal equilibrium must exist. Static solutions for the energy balance have been derived (Rosner, Tucker, and Vaiana 1978; Craig, McClymont, and Underwood 1978; Vesecky, Antiochos, and Underwood 1979), and the linear stability of these equilibria have been investigated in several papers (Antiochos 1979; Hood and Priest 1980; Chiuderi, Einaudi, and Torricelli-Ciamponi 1981; Craig and McClymont 1981). The contradictory results of some stability studies evidenced the crucial role of the corona-chromosphere interaction on the coronal stability (McClymont and Craig 1985a, b; Antiochos *et al.* 1985).

Much has been investigated about chromospheric evaporation (Doschek *et al.* 1986), and references therein) as a stabilizing effect during solar flares. It seems reasonable to assume that this mechanism also operates in nonflaring regions as a response to coronal perturbations. Moreover, Craig and McClymont (1987) had recently shown that this mechanism is essential in stabilizing the thermal evolution of coronal loops. Kuin and Martens (1982) developed an interesting model in which the evaporation-condensation mechanism is shown to stabilize the linearly unstable evolutions. There was a free parameter in their model (control parameter), defined as an efficiency of the chromosphere-corona coupling, whose reduction below a critical value implies the instability of the static solution and the emergence of a stable limit cycle. A criticism can be made at this point, because this efficiency is a completely free parameter and no attempt has been made to estimate its typical values, it may well be possible that the typical range of variation lies within the zone, where the static solution is stable (Craig and Schulkes 1985).

In a previous paper (Gómez, Sicardi Schifino, and Ferro Fontán 1990, hereafter Paper I) we derived from the hydrodynamic equations a simplified model described through two

ordinary nonlinear equations that predict the evolution of mean coronal pressure and density:

$$\partial_t \delta n = \frac{1}{1 + \delta p} \left\{ \alpha \delta T + \beta \frac{h}{\theta} [1 - (1 + \delta p)^{\gamma_b + 2}] \right\}, \quad (1.1a)$$

$$\partial_t \delta p = 1 - (1 + \delta p)^2 (1 + \delta T)^\gamma + \frac{5}{3} \beta h [1 - (1 + \delta p)^{\gamma_b + 2}] + \frac{5}{3e} \alpha \theta \delta T, \quad (1.1b)$$

where

$$\delta T = (\delta p - \delta n)/(1 + \delta n), \quad (1.2a)$$

$$\alpha = \frac{3}{5} \frac{e}{e - 1} \frac{K_0 T_{ob}^{3/2} T_0^2}{EL^2 h}, \quad \beta = \frac{3}{5} \frac{e}{e - 1} \frac{1}{1 - \gamma^*}, \quad (1.2b)$$

$t$  is a dimensionless time (in units of  $3P_0/2E$ ),  $h = L_b/L$ , and  $\theta = T_{ob}/T_0$  are dimensionless functions of  $E$  (of order  $\ll 1$ ), and  $\gamma$  and  $\gamma_b$  are exponents of the radiative loss function at coronal and chromospheric temperatures respectively. The parameter  $\gamma^*$  measures an assumed spatial discontinuity in the heating rate ( $\gamma^* = [E_b - E]/E_b$ , where  $E_b$  is heating rate at the base). We denote by  $\delta n$ ,  $\delta p$ , and  $\delta T$  the relative departures from the static equilibrium of density, pressure, and temperature respectively,  $E$  is the coronal heating rate,  $L$  is the half-length of the loop, and  $L_b$  is the width of the base (column of the upper chromosphere which effectively interacts with the corona).  $K_0$  is the conductivity coefficient of Spitzer (1962) and  $T_0$ ,  $T_{ob}$ , and  $P_0$  are the equilibrium coronal temperature, chromospheric temperature, and pressure, respectively. The coupling to the chromosphere was properly modeled and the coronal heating rate acts as the control parameter of the model. We have shown through a linear stability analysis of these equations that below a critical heating rate of  $1.4 \times 10^{-3}$  ergs  $\text{cm}^{-3} \text{s}^{-1}$  (for a typical loop of half-length  $3 \times 10^9$  cm), and  $\gamma^* = 0.05$ , the static equilibrium becomes unstable, spiral-

ing out of this solution with a period of about 30 minutes. No qualitative changes appear when the free parameter  $\gamma^*$  is varied in the range  $0 < \gamma^* \leq 1$ .

Our global description of coronal loops through spatially averaged quantities is justified by the effect of thermal conductivity in smoothening small-scale perturbations (see also Craig and McClymont 1987). Moreover, in a recent paper, Pakkert, Martens, and Verhulst (1987) show that limit cycles seem to be contained among the solutions of the full set of hydrodynamic equations.

As is well known, there are no general methods for solving nonlinear equations. However, much progress has been made during the last few years, and many applications of nonlinear methods to astrophysical problems have been developed (see Martens 1984 for a review). In this paper, we study the nonlinear stability of equation (1.1) both analytically and numerically. The aim of this study is to search for new equilibrium branches capable of attracting the linearly unstable evolutions. The analytical work was performed following a perturbative expansion of the equations around the critical point in powers of a small parameter defined as the limit cycle amplitude. We developed equation (1.1) up to fifth order and found that a subcritical Hopf bifurcation takes place at the critical heating rate. In § IIa, we detail the general method employed, and in § IIb, we apply it to the problem under study. The perturbative method has been adapted so that not only the new equilibrium branches can be found, but also the relaxation of the system to the stable ones. In § III, we describe the results of the numerical integration of equation (1.1), and in § IV, we discuss how our analytic and numerical results compare and how our model compares with that of Kuin and Martens (1982). Finally, we attempt the explanation of some observed features through the existence of limit cycle solutions.

## II. PERTURBATIVE ANALYSIS

### a) General Method

We shall describe now the perturbative technique applied to obtain the asymptotic solution of a set of nonlinear equations near a bifurcation point. While this method has been essentially based on Iooss and Joseph (1980), we have generalized it in order to obtain not only the equilibrium branches but also the nonlinear relaxation toward the stable ones.

Given a problem that can be described by a two-dimensional vector field  $\mathbf{u}$  which evolves in time according to

$$\partial_t \mathbf{u}_i = \mathcal{F}_i(\mathbf{u}, E), \quad (2.1)$$

where  $E$  is a control parameter, the static equilibria are those  $\mathbf{u}_0(E)$  which solve

$$\mathcal{F}_i[\mathbf{u}_0(E), E] = 0. \quad (2.2)$$

Performing a linearization of equation (2.1) around  $\mathbf{u}_0(E)$ , the stability of these equilibria for each value of  $E$  can be found. Whenever the sign of the real part of one of the eigenvalues of the matrix  $\partial_j \mathcal{F}_i[\mathbf{u}_0(E), E]$  becomes positive, the equilibrium  $\mathbf{u}_0(E)$  turns unstable. If the pair of eigenvalues is complex conjugate, a Hopf bifurcation arises for each  $E_*$  where the real part of the eigenvalues changes its sign. Hereafter, we shall restrict ourselves to the study of this type of bifurcation. As usual, we write down equation (2.1) in local form:

$$\partial_t \psi_i = \mathcal{F}_i(\psi, \mu), \quad (2.3a)$$

where the new vector field is

$$\psi = \mathbf{u} - \mathbf{u}_0(E), \quad (2.3b)$$

and the control parameter is replaced by

$$\mu = (E_* - E)/E_*. \quad (2.3c)$$

Since we are interested in a search of new equilibria close to  $\mathbf{u}_0(E)$ , we can work with the first terms of the Taylor expansion of the function  $\mathcal{F}_i$  around  $\psi_i = 0$  ( $i = 1, 2$ ). Thus,

$$\partial_t \psi_i = \sum_{n=1}^{\infty} \frac{1}{n!} \partial_{j_1, \dots, j_n}^{(n)} \mathcal{F}_i[\mathbf{u}_0(E), E] \psi_{j_1} \dots \psi_{j_n}, \quad (2.4)$$

where the sum convention for the  $j_k = 1, 2$  has been applied. As we will see below, we must retain in our model equation (1.1) up to the fifth-order term to get a new stable (however nonstatic) equilibrium in the linearly unstable cases.

As we have stated earlier (see also Paper I, § IV), the eigenvalues of  $L_{ij} = \partial_j \mathcal{F}_i$  are complex conjugate

$$\lambda = \xi + i\eta = \frac{L_{11} + L_{22}}{2} + i \sqrt{L_{11}L_{22} - L_{12}L_{21} - \frac{(L_{11} + L_{22})^2}{4}}. \quad (2.5)$$

At the bifurcation point ( $E = E_*$ ), the trace of  $L$  changes sign (for  $E < E_*$ , the trace becomes positive, implying instability) while the determinant remains positive. The eigenvectors are

$$L \cdot \zeta = \lambda \cdot \zeta, \quad (2.6)$$

and

$$L^T \cdot \zeta^* = \lambda^* \zeta^*, \quad (2.7)$$

where  $L^T$  is the adjoint of  $L$  and  $\zeta^*$  is the eigenvector of the adjoint problem. These eigenvectors satisfy the following orthonormal relations:

$$\zeta_k \zeta_k^* = 1, \quad (2.8a)$$

$$\zeta_k \zeta_k = 0, \quad (2.8b)$$

and they can be expressed in terms of the  $L$  components (evaluated at the critical point) as

$$\zeta = \frac{1}{1 + (\lambda - L_{11})/(-L_{12}L_{21})^{1/2}} \begin{pmatrix} 1 \\ \frac{\lambda - L_{11}}{L_{12}} \end{pmatrix}, \quad (2.9a)$$

$$\zeta^* = \frac{-1}{1 + (\lambda + L_{11})/(-L_{12}L_{21})^{1/2}} \begin{pmatrix} 1 \\ \frac{\lambda + L_{11}}{L_{21}} \end{pmatrix}. \quad (2.9b)$$

Given that  $\zeta$  and  $\zeta^*$  are independent eigenvectors, any real vector  $\psi$  can be decomposed as

$$\psi_i = a(t)\zeta_i + a^*(t)\zeta_i^*. \quad (2.10)$$

In a completely general way, we can substitute equation (2.10) into equation (2.4) and use the orthonormal relations (2.8) to obtain an evolution equation for the amplitude  $a(t)$ :

$$\partial_t a = \sum_{n=1}^{\infty} \sum_{k=0}^n \binom{n}{k} \sigma_k^{(n)} a^{n-k} (a^*)^k, \quad (2.11)$$

where

$$\sigma_k^{(n)} = \frac{1}{n!} \partial_{j_1, \dots, j_n}^{(n)} \mathcal{F}_i \zeta_i^* \zeta_{j_1}^* \dots \zeta_{j_k}^* \zeta_{j_{k+1}} \dots \zeta_{j_n}. \quad (2.12)$$

We shall now look for small-amplitude limit cycle solutions in the neighborhood of the bifurcation point. Thus, we expand variables and control parameter in powers of a small parameter  $\epsilon$ :

$$a(t) = A(t) \sum_{k=1}^{\infty} a_k(s) \epsilon^k, \quad s = \omega(\epsilon)t, \quad (2.13a)$$

$$\omega(\epsilon) = \omega_0 + \sum_{k=1}^{\infty} \omega_{2k} \epsilon^{2k}, \quad (2.13b)$$

$$\partial_t A = \sum_{k=1}^{\infty} A'_{2k} \epsilon^{2k}, \quad (2.13c)$$

$$\mu(\epsilon) = \sum_{k=1}^{\infty} \mu_{2k} \epsilon^{2k}, \quad (2.13d)$$

and we define  $\epsilon$  as the amplitude of the limit cycle

$$\epsilon = \frac{1}{2\pi A} \int_0^{2\pi} ds e^{-is} a = [a]. \quad (2.14)$$

Notice that  $A(t)$  is a slowly varying function of  $t(\partial_t A \propto \epsilon^2)$  and thus the time integral in equation (2.14) can be performed assuming  $A = \text{constant}$ . Moreover,  $A$  is defined so that  $A \rightarrow 1$  for  $t \rightarrow \infty$ , recovering at that limit the expressions of Iooss and Joseph (1980). We note also that for Hopf bifurcations  $\omega$ ,  $\partial_t A$  and  $\mu$  are even functions of  $\epsilon$  (see eqs. [2.13b]–[2.13d]) as has been rigorously proved (Hassard, Kazarinoff, and Wan 1981).

Equation (2.11) transforms into an equality between polynomials in  $\epsilon$ , and thus it must hold at any order in  $\epsilon$ . To first order,

$$\omega_0 \partial_s a_1 = i\eta_* a_1, \quad (2.15)$$

where hereinafter the subscript “\*” means that the function is evaluated at the bifurcation point. We choose  $\omega_0 = \eta_*$ , and thus

$$a_1 = a_{10} e^{is}. \quad (2.16)$$

According to equation (2.14), we have  $[a_1] = a_{10} = 1$ . To second order,

$$\omega_0 A(\partial_s a_2 - ia_2) = \sigma_0^{(2)} A^2 a_1^2 + 2\sigma_1^{(2)} |A|^2 + \sigma_2^{(2)} (A^* a_1^*)^2. \quad (2.17)$$

The condition (2.14) is automatically satisfied by equation (2.17). Notice that for any  $k > 1$ , condition (2.14) reads  $[a_k] = 0$  and implies that equations of the type of (2.17) can be solved whenever the right-hand side has no terms proportional to  $e^{is}$ . This solvability condition, also known as the Fredholm alternative, when applied to the different orders in  $\epsilon$ , will provide equations from which  $\omega_{2k}$ ,  $A'_{2k}$ , and  $\mu_{2k}$  can be obtained. Following to higher orders in  $\epsilon$ , we find

$$\omega_0 A(\partial_s a_k - ia_k) = \sum_{j=-k/2}^{k/2} \Lambda_{2j}^{(k)}(A, A^*) e^{2ijs}, \quad (2.18)$$

where the solvability condition implies  $\Lambda_1^{(k)} = 0$ . The expressions of the  $\Lambda_j^{(k)}$ 's up to  $k = 4$  are given in the Appendix. Equation (2.18) can be readily solved, obtaining

$$a_k(s) = \frac{1}{i\omega_0 A} \sum_{j=-k/2}^{k/2} \Lambda_{2j}^{(k)}(A, A^*) \frac{e^{2ijs}}{2j-1}. \quad (2.19)$$

For even values of  $k$ , the condition  $\Lambda_1^{(k)} = 0$  is automatically satisfied, while for odd values, the solvability condition can be

written formally as

$$\frac{A'_{2k}}{A} = \Gamma^{(2k)} - \sum_{j=1}^k \Gamma_{2j}^{(2k)} |A|^{2j}, \quad (2.20a)$$

where

$$\Gamma^{(2k)} = \sum_{j=1}^k \Gamma_{2j}^{(2k)}, \quad (2.20b)$$

because of the condition  $A \rightarrow 1$  for  $t \rightarrow \infty$ . The explicit expression for the coefficients  $\Gamma_j^{(2)}$  and  $\Gamma_j^{(4)}$  is shown in the Appendix.

The evolution equation for the slowly varying amplitude  $A$  is thus

$$\partial_t A = \sum_{k=1}^{\infty} \Gamma^{(2k)} \epsilon^{2k} A - \sum_{k=1}^{\infty} \sum_{j=1}^k \Gamma_{2j}^{(2k)} |A|^{2j} \epsilon^{2k} A, \quad (2.21)$$

and it is readily verified that

$$\sum_{k=1}^{\infty} \Gamma^{(2k)} \epsilon^{2k} = \lambda - i\omega = \xi + i(\eta - \omega). \quad (2.22)$$

It is also straightforward to construct a function to analyze the stability to the limit cycle solution. Decomposing the  $\Gamma$ 's and  $A$  as

$$\Gamma_{2j}^{(2k)} = \gamma_{2j}^{(2k)} + i\gamma'_{2j}^{(2k)}, \quad (2.23a)$$

$$A = |A| e^{i\phi}, \quad (2.23b)$$

and taking the real part of equation (2.21), we obtain

$$\partial_t |A| = \xi |A| - \sum_{k=1}^{\infty} \sum_{j=1}^k \gamma_{2j}^{(2k)} |A|^{2j+1} \epsilon^{2k}. \quad (2.24)$$

We can write down this equation in the form

$$\partial_t |A| = -\frac{\partial S}{\partial |A|}, \quad (2.25)$$

where

$$S(|A|) = -\frac{\xi}{2} |A|^2 + \sum_{k=1}^{\infty} \sum_{j=1}^k \gamma_{2j}^{(2k)} \frac{|A|^{2j+2}}{2j+2} \epsilon^{2k}, \quad (2.26)$$

is a generalized potential in the sense that the equilibria of the system correspond to the extrema of this function being the minima of the stable ones (Haken 1983). This is so because equation (2.25) implies  $\partial_t S \leq 0$  for all values of  $|A|$ .

### b) Application to the Model Equations

For the case of equation (1.1), the vector field  $\psi$  and the control parameter  $\mu$  can be defined as

$$\psi_1 = \delta n, \quad \psi_2 = \delta p, \quad (2.27)$$

$$\mu = (E_* - E)/E_*, \quad (2.28)$$

so that the static equilibrium is linearly unstable for  $\mu > 0$ .

In order to find new stable solutions of equation (1.1), it was necessary to expand these equations up to fifth order, as will be seen below. The first nontrivial solvability condition appears at order  $\epsilon^3$ , where expression (2.20a) reads

$$\frac{A'_2}{A} = \Gamma^{(2)} - \Gamma_2^{(2)} |A|^2, \quad (2.29)$$

where

$$\Gamma^{(2)} = \mu_2 \partial_\mu \lambda - i\omega_2, \quad (2.30)$$

$$\Gamma_2^{(2)} = \frac{2\sigma_0^{(2)}\sigma_1^{(2)} - 4|\sigma_1^{(2)}|^2 - (2/3)|\sigma_2^{(2)}|^2}{i\omega_0} - 3\sigma_1^{(3)}, \quad (2.31)$$

as has also been written in the Appendix. Imposing the condition (2.20b), we can obtain numerical values for  $\mu_2$  and  $\omega_2$ :

$$\mu_2 = -5.1, \quad \omega_2 = -17.4, \quad (2.32)$$

and also

$$\gamma^{(2)} = \gamma_2^{(2)} = -0.29. \quad (2.33)$$

On one side, the fact that  $\mu_2 < 0$  implies that a new equilibrium branch  $\mu = \mu_2 \epsilon^2$  appears for negative values of the control parameter. On the other hand, looking at equation (2.26) we realize that the generalized potential at order  $\epsilon^3$  results in

$$S \cong -\frac{\gamma^{(2)}}{2} \epsilon^2 |A|^2 \left(1 - \frac{1}{2} |A|^2\right). \quad (2.34)$$

This function has two extrema: a minimum at  $|A| = 0$  indicating that the static equilibrium is stable, and a maximum at  $|A| = 1$  showing that the new equilibrium branch is unstable. This kind of behavior is typical of the subcritical bifurcations (see Fig. 1b) as opposed to the supercritical bifurcations (Fig. 1a), where a new stable branch appears just when the static equilibrium turns unstable.

At order  $\epsilon^5$ , the condition  $\Lambda_1^{(5)} = 0$  reads

$$\frac{A_4'}{A} = \Gamma^{(4)} - \Gamma_2^{(4)} |A|^2 - \Gamma_4^{(4)} |A|^4, \quad (2.35)$$

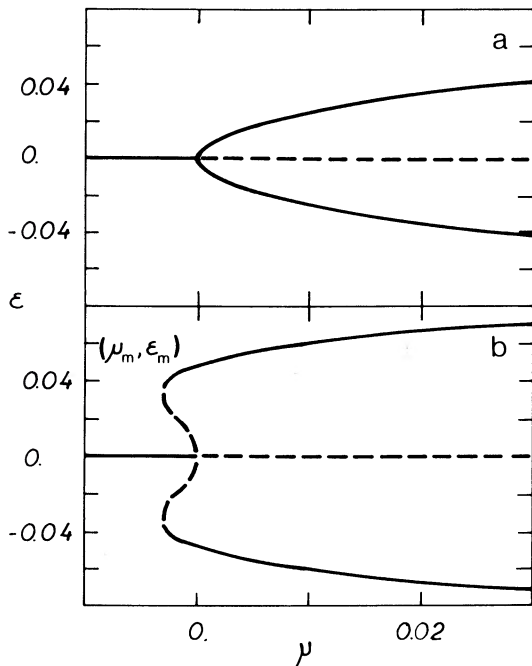


FIG. 1.—(a) Supercritical Hopf bifurcation. (b) Subcritical Hopf bifurcation perturbatively derived from our equations. Dotted lines represent unstable equilibria.

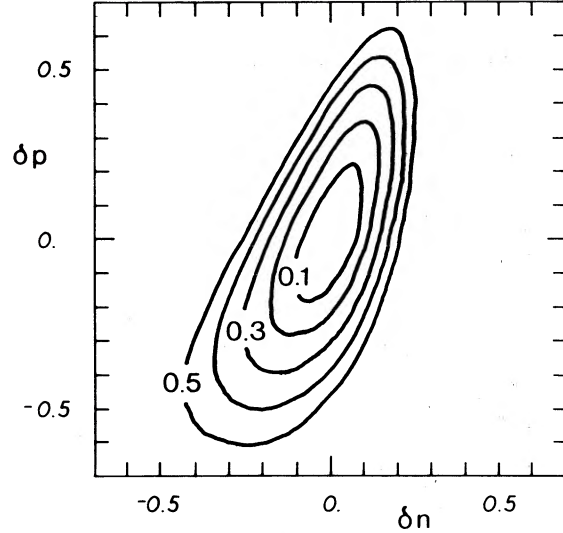


FIG. 2.—Limit cycles (labeled by the corresponding value of  $\mu$ ) obtained through numerical integration of our equations.

where the expression for  $\Gamma^{(4)}$ ,  $\Gamma_2^{(4)}$ , and  $\Gamma_4^{(4)}$  is shown in the Appendix. The  $S$  function up to fifth order is

$$S(|A|) = -\frac{1}{2}[\gamma^{(2)}\epsilon^2 + \gamma^{(4)}\epsilon^4] |A|^2 + \frac{1}{4}[\gamma_2^{(2)}\epsilon^2 + \gamma_2^{(4)}\epsilon^4] |A|^4 + \frac{1}{6}\gamma_4^{(4)}\epsilon^4 |A|^6, \quad (2.36)$$

where

$$\gamma_2^{(4)} = -7.9, \quad \gamma_4^{(4)} = 131.7. \quad (2.37)$$

The new equilibrium branch is described now by  $\mu = \mu_2 \epsilon^2 + \mu_4 \epsilon^4$ , where

$$\mu_4 = 2197.6, \quad (2.38)$$

by application of condition (2.20b). Since  $S(|A|)$  is a function of  $\epsilon$  and in turn  $\epsilon = \epsilon(\mu)$ , the stability of the new equilibria can change as the control parameter  $\mu$  is varied. The results of the stability analysis are shown in Figure 1b, where the dotted line indicates unstable equilibria. Using the definitions (2.10) and (2.13a) and the solutions (2.19) for  $k \leq 4$ , the trajectory of the system in the  $(\delta n, \delta p)$  plane can be constructed. We have verified that these trajectories compare fairly well with our numerical trajectories (like those shown in Fig. 2) provided the parameter  $\mu$  is sufficiently close to the bifurcation point ( $\mu = 0$ ). For  $\mu > 0.2$ , the perturbative trajectories become too small compared with those derived numerically.

We can study how the relaxation time depends on the control parameter  $\mu$  by analytically integrating equation (2.24) for  $k \leq 4$ . In Figure 3, we show  $|A(t)|$  for different values of  $\mu$ , normalizing in each case to the corresponding  $\delta p_{\max}$  for the sake of comparison with numerical results (dots in Fig. 3).

### III. NUMERICAL RESULTS

We have solved equations (1.1) and (1.1b) numerically using a fourth-order Runge Kutta method, for different values of  $\mu$  and initial conditions. In figure 2, we plotted the limit cycle solutions, each one labeled by the corresponding value of  $\mu$ .

To test the relaxation toward the limit cycles shown in Figure 2, we computed each crossing of the trajectory with the  $\delta n = 0, \delta p > 0$  semi-axis both from initial conditions outside and inside the attractor, as can be seen in Figure 3 (dots). The

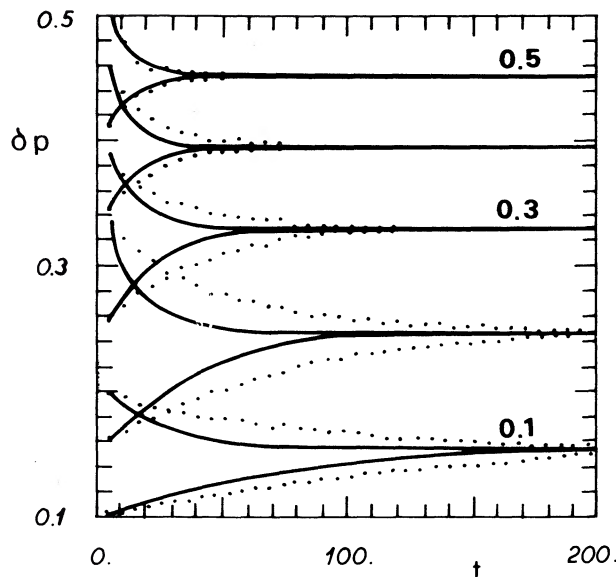


FIG. 3.—Relaxation toward the stable limit cycles for different values of the control parameter  $\mu$  (see label). Continuous lines correspond to the analytic evolution of  $A(t)$  normalized (with  $\delta p_{\max}$ ), while dots indicate the successive crossings of the trajectory through the positive part of the  $\delta p$  axis. The temporal separation between dots coincides with the limit cycle period.

temporal separation between dots in Figure 3 asymptotically approaches the period of the corresponding limit cycle.

For the radiative loss function, we have used the piecewise power law given in equation (2.4) of Paper I, which is a matching between the function given by Peres *et al.* (1982) for the chromosphere with the fit of Craig and McClymont (1986) for the transition region and corona.

It is important to note the quite slow relaxation time of the system for control parameter values sufficiently close to the critical point. In fact, we can see from equation (2.24) that the relaxation time behaves like  $\xi^{-1}$  and consequently goes to infinity at the bifurcation point. According to this general result, we believe that the two stable limit cycles found by Craig and Schulkes (1985, see their Fig. 3a) for the Kuin and Martens (1982) equations at  $\mu = 0$  might not be real, but a consequence of the very slow relaxation at this point.

In Figure 4, we display the temporal evolution of temperature perturbation for the limit cycle corresponding to  $\mu = 0.5$ . A certain preference of the system to lie in the upper part of the cycle can be noticed, as has also been reported by Kuin and Martens (1982). We calculated the mean value of  $\delta T(t)$  over one period and obtained 0.16, thus indicating that the measured temperature should be 16% above  $T_0$ , provided that this limit cycle solution is operative in a bundle of magnetic field lines with their phases evenly distributed (see Paper I).

#### IV. DISCUSSION

The aim of this paper has been to complement the results of Paper I, performing an analytical (however approximative) and numerical integration of equation (1.1). As has been found in Paper I, for heating rate values lower than  $E_*$ , the static equilibrium turns unstable. In this paper, we study the characteristics of the new equilibria which appear at the critical point.

As a rule, we find that for the same value of the control parameter, our limit cycles have amplitudes much smaller than

those found by Kuin and Martens (1982). The smallness of the limit cycles reflects the ability of the upper chromosphere to react against instabilities of the coronal plasma and effectively saturate them through the evaporation-condensation mechanism. The relatively low amplitude limit cycles we have obtained might not imply observable consequences on the temperature and density of the loop. For example, we have shown above that for the limit cycle corresponding to  $\mu = 0.5$ , the measured temperature will be 16% in excess of  $T_0$  (due to asymmetries of the cycle) and constant in time. This enhancement may probably fall within the error range of the measurement. Whether or not larger amplitude oscillatory behavior exists cannot be decided from our equations due to our assumption of thinness of the conductively influenced region (see Paper I).

The fact that the Hopf bifurcation we found is of the subcritical type (Fig. 1b) implies, aside of the cyclic behavior, the occurrence of catastrophes when  $\mu$  changes from negative to positive and the system lies in the static equilibrium (and also when the system is in the limit cycle branch and  $\mu$  is reduced below the minimum  $\mu$  for this branch). However, again due to the very low values of  $\mu_m$  and  $\epsilon_m$ , the observational consequences of this catastrophe can be completely neglected. Moreover, if we add white noise terms to equation (1.1) in order to somehow take into account the complex interaction of the system under study with their surroundings, we realize that the very concept of bifurcation point becomes meaningless and must be replaced by the notion of bifurcation region (see Meunier and Verga 1988 for a detailed description of the action of noise on bifurcating solutions). When noise is present, the deterministic description of the problem is substituted by a probabilistic one. Sufficiently close to the bifurcation point, the probabilities of finding the system in the static or in the limit cycle equilibria become comparable, where the extension of this bifurcation region is determined by the level of noise present. An observable consequence of the addition of noise to our model could be the extra Doppler widening of EUV lines caused by the superposition of transient evaporation-condensation processes driven by noise.

However, assuming the existence of relatively low amplitude

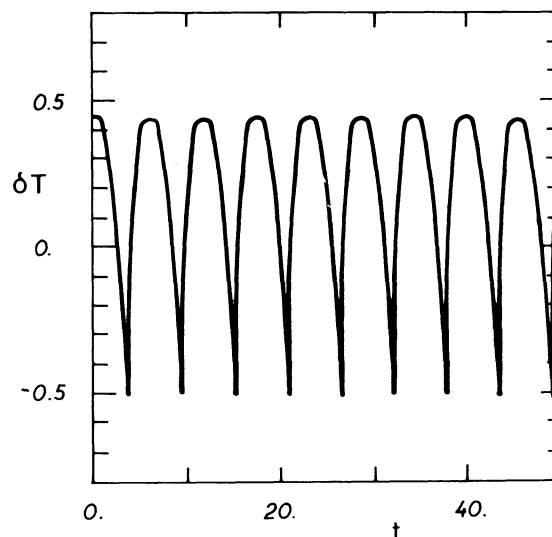


FIG. 4.—Temporal behavior of temperature for  $\mu = 0.5$

limit cycles (see Fig. 4 of Paper I), we are able to explain the nonthermal Doppler widths of EUV lines forming in the transition region. Moreover, if we assume that the heating mechanism is Joule dissipation of magnetic energy continuously replenished by subphotospheric convection (see Paper I), we can also explain the observed narrowing of these lines in certain active regions like quiescent prominences and sunspots (Cheng, Doschek, and Feldman 1976; Feldman and Doschek 1977). This result comes from the fact that  $E \propto (B_0/L)^2$  ( $B_0$  is the magnetic field along the loop and  $L$  is its half-length) and  $E_* \propto L^{-2}$ . Thus, the condition for the existence of limit cycles

( $E < E_*$ ) poses an upper limit for the magnetic field value, above which the cyclic solution turns off.

We gratefully acknowledge M. Machado for very useful comments and suggestions. This work was supported by the Consejo Nacional de Investigaciones Científicas y Técnicas (CONICET, Argentina) under Grant 9069/03 and by the University of Buenos Aires under Grant 097-EX. One of us (D. G) has been honored with a fellowship of CONICET, and C. F. F. is a member of the Carrera del Investigador Científico (CONICET).

## APPENDIX

EXPRESSIONS OF COEFFICIENTS  $\Lambda$  AND  $\Gamma$ 

$$\Lambda_{-3}^{(3)} = \left\{ \sigma_3^{(3)} - \frac{2}{3i\omega_0} (\sigma_1^{(2)}\sigma_2^{(2)} + 3\sigma_0^{(2)*}\sigma_1^{(2)}) \right\} (A^*)^3,$$

$$\Lambda_{-1}^{(3)} = \left[ 3\sigma_2^{(3)} - \frac{2}{3i\omega_0} \{ \sigma_0^{(2)}\sigma_2^{(2)} + 3\sigma_0^{(2)*}\sigma_1^{(2)} + 6[\sigma_1^{(2)}]^2 - 6\sigma_1^{(2)*}\sigma_2^{(2)} \} \right] |A|^2 A^*,$$

$$\Lambda_3^{(3)} = \left[ \sigma_0^{(3)} + \frac{2}{3i\omega_0} \{ 3[\sigma_0^{(2)}]^2 + \sigma_1^{(2)}\sigma_2^{(2)*} \} \right] A^3,$$

$$\Lambda_{-4}^{(4)} = \left[ \sigma_4^{(4)} - \frac{1}{6i\omega_0} [2\sigma_2^{(3)}\sigma_0^{(2)} + 18\sigma_3^{(3)}\sigma_0^{(2)*} + 3\sigma_1^{(2)}\Lambda_{-3}^{(3)} + 6\sigma_2^{(2)}\Lambda_3^{(3)*}] - \frac{\sigma_2^{(2)}}{9\omega_0^2} \{ \sigma_0^{(2)}\sigma_2^{(2)} + 9[\sigma_0^{(2)*}]^2 + 6\sigma_0^{(2)*}\sigma_1^{(2)} \} \right] (A^*)^4,$$

$$\Lambda_{-2}^{(4)} = \left[ \mu_2 \partial_\mu \sigma_2^{(2)} - \frac{\omega_2}{\omega_0} \sigma_2^{(2)} \right] (A^*)^2 + \left[ 4\sigma_3^{(4)} - \frac{1}{6i\omega_0} \{ 2\sigma_2^{(2)}\Gamma_2^{(2)} + 4\sigma_1^{(3)}\sigma_2^{(2)} + 12\sigma_2^{(3)}[\sigma_1^{(2)} + \sigma_0^{(2)*}] - 36\sigma_3^{(3)}\sigma_1^{(2)*} + 3\sigma_0^{(2)}\Lambda_{-3}^{(3)} \right. \\ \left. + 6\sigma_1^{(2)}[\Lambda_{-1}^{(3)} + \Lambda_3^{(3)*}] \right] + \frac{1}{3\omega_0^2} \{ 6\sigma_0^{(2)*}\sigma_1^{(2)*}\sigma_2^{(2)} + 4|\sigma_1^{(2)}|^2\sigma_2^{(2)} - 2\sigma_0^{(2)}\sigma_1^{(2)}\sigma_2^{(2)} - 4\sigma_0^{(2)*}[\sigma_1^{(2)}]^2 \} |A|^2 (A^*)^2$$

$$\Lambda_0^{(4)} = 2 \left[ \mu_2 \partial_\mu \sigma_1^{(2)} - \frac{\omega_2}{\omega_0} \sigma_1^{(2)} \right] |A|^2 + \left[ 6\sigma_2^{(4)} - \frac{1}{i\omega_0} [2\sigma_1^{(2)}\Gamma_2^{(2)} + \sigma_0^{(3)}\sigma_2^{(2)} + \sigma_1^{(3)}\sigma_0^{(2)*} + 4\sigma_1^{(3)}\sigma_1^{(2)} - \sigma_2^{(3)}\sigma_0^{(2)} - 4\sigma_2^{(3)}\sigma_1^{(2)*} \right. \\ \left. - \sigma_3^{(3)}\sigma_2^{(2)*} + \sigma_0^{(2)}\Lambda_{-1}^{(3)} - \sigma_2^{(2)}\Lambda_{-1}^{(3)*} \right] + \frac{1}{3\omega_0^2} \left\{ [\sigma_0^{(2)}]^2\sigma_2^{(2)} - 12\sigma_0^{(2)}[\sigma_1^{(2)}]^2 + \sigma_0^{(2)*}|\sigma_2^{(2)}|^2 - 12[\sigma_1^{(2)*}]^2\sigma_2^{(2)} \right. \\ \left. + 6\sigma_1^{(2)} \left[ |\sigma_0^{(2)}|^2 + 4|\sigma_1^{(2)}|^2 + \frac{1}{9}|\sigma_2^{(2)}|^2 \right] \right\} |A|^4,$$

$$\Lambda_2^{(4)} = \left[ \mu_2 \partial_\mu \sigma_0^{(2)} - \frac{\omega_2}{\omega_0} \sigma_0^{(2)} \right] A^2 + \left[ 4\sigma_1^{(4)} - \frac{1}{6i\omega_0} \{ 36\sigma_0^{(3)}\sigma_1^{(2)} - 6\sigma_0^{(2)}\Gamma_2^{(2)} - 3\sigma_1^{(3)}\sigma_1^{(2)*} - 12\sigma_1^{(3)}\sigma_0^{(2)} - 2\sigma_2^{(3)}\sigma_2^{(2)*} \right. \\ \left. - 3\sigma_2^{(2)}\Lambda_{-3}^{(3)*} - 6\sigma_1^{(2)}[\Lambda_3^{(3)} + \Lambda_{-1}^{(3)*}] \right] + \frac{1}{3\omega_0^2} \{ 6[\sigma_0^{(2)}]^2\sigma_1^{(2)} - 2\sigma_1^{(2)*}|\sigma_2^{(2)}|^2 + 4[\sigma_1^{(2)}]^2\sigma_2^{(2)*} - 12\sigma_0^{(2)}|\sigma_1^{(2)}|^2 \} |A|^2 A^2,$$

$$\Lambda_4^{(4)} = \left[ \sigma_0^{(4)} + \frac{1}{6i\omega_0} [18\sigma_0^{(3)}\sigma_0^{(2)} + 2\sigma_1^{(3)}\sigma_2^{(2)*} + 6\sigma_0^{(2)}\Lambda_3^{(3)} + 3\sigma_1^{(2)}\Lambda_{-3}^{(3)*}] - \frac{1}{9\omega_0^2} \{ 9[\sigma_0^{(2)}]^3 + |\sigma_2^{(2)}|^2\sigma_2^{(2)*} + 6\sigma_0^{(2)}\sigma_1^{(2)}\sigma_2^{(2)*} \} \right] A^4,$$

$$\Gamma^{(2)} = \mu_2 \partial_\mu \lambda - i\omega_2, \quad \Gamma_2^{(2)} = \frac{2\sigma_0^{(2)}\sigma_1^{(2)} - 4|\sigma_1^{(2)}|^2 - (2/3)|\sigma_2^{(2)}|^2}{i\omega_0} - 3\sigma_1^{(3)},$$

$$\Gamma^{(4)} = \frac{1}{2}\mu_2^2 \partial_\mu^2 \lambda + \mu_4 \partial_\mu \lambda - i\omega_4,$$

$$\Gamma_2^{(4)} = \frac{2}{i\omega_0} \left\{ 2\sigma_0^{(2)} \left[ \mu_2 \partial_\mu \sigma_1^{(2)} - \frac{\omega_2}{\omega_0} \sigma_1^{(2)} \right] - 2\sigma_1^{(2)} \left[ \mu_2 \partial_\mu \sigma_1^{(2)} - \frac{\omega_2}{\omega_0} \sigma_1^{(2)} \right]^* - \sigma_1^{(2)} \left[ \mu_2 \partial_\mu \sigma_0^{(2)} - \frac{\omega_2}{\omega_0} \sigma_0^{(2)} \right] - \frac{1}{3} \sigma_2^{(2)} \left[ \mu_2 \partial_\mu \sigma_2^{(2)} - \frac{\omega_2}{\omega_0} \sigma_2^{(2)} \right]^* \right\},$$

$$\begin{aligned}
\Gamma_4^{(4)} = & -\Gamma_2^{(4)} - 10\sigma_2^{(5)} + \frac{2}{i\omega_0} \left[ \sigma_0^{(2)}\Lambda_0^{(4)} - \sigma_1^{(2)}[\Lambda_0^{(4)*} + \Lambda_2^{(4)}] - \frac{1}{3}\sigma_2^{(2)}\Lambda_{-2}^{(4)*} + \frac{3}{4} \left\{ \sigma_0^{(3)}\Lambda_{-1}^{(3)} - \sigma_2^{(3)}[\Lambda_3^{(3)} + 2\Lambda_{-1}^{(3)*}] - \frac{1}{2}\sigma_3^{(3)}\Lambda_{-3}^{(3)*} \right\} \right. \\
& + \frac{2}{3}\sigma_0^{(4)}\sigma_2^{(2)} + 2\sigma_1^{(4)}\sigma_0^{(2)*} + 12\sigma_1^{(4)}\sigma_1^{(2)} - 12\sigma_2^{(4)}\sigma_1^{(2)*} - 6\sigma_2^{(4)}\sigma_0^{(2)} - 2\sigma_3^{(4)}\sigma_2^{(2)*} \left. \right] - \frac{1}{\omega_0^2} \left[ \sigma_0^{(2)} \left[ \sigma_0^{(2)}\Lambda_{-1}^{(3)} + \frac{1}{3}\sigma_2^{(2)}\Lambda_3^{(3)} \right] \right. \\
& + 2\sigma_1^{(2)} \left\{ \frac{1}{2}\sigma_0^{(2)*}\Lambda_3^{(3)} + \sigma_1^{(2)}\Lambda_{-1}^{(3)*} + \frac{1}{12}\sigma_2^{(2)}[\Lambda_{-3}^{(3)*} + 2\Lambda_{-1}^{(3)}] \right\} + 2\sigma_2^{(2)} \left[ \frac{1}{4}\sigma_0^{(2)*}\Lambda_{-3}^{(3)} - \sigma_1^{(2)*}\Lambda_{-1}^{(3)*} \right] + \sigma_0^{(3)}\{\sigma_0^{(2)}\sigma_2^{(2)} \\
& - 12[\sigma_1^{(2)}]^2\} - 6\sigma_1^{(3)} \left[ |\sigma_0^{(2)}|^2 + 4|\sigma_1^{(2)}|^2 + \frac{1}{9}|\sigma_2^{(2)}|^2 + \sigma_0^{(2)}\sigma_1^{(2)} \right] + \sigma_2^{(3)}\{\sigma_0^{(2)}\sigma_2^{(2)} - 12[\sigma_1^{(2)}]^2 \\
& + 4\sigma_1^{(2)*}\sigma_2^{(2)} - 12\sigma_0^{(2)*}\sigma_1^{(2)*}\} - 2\sigma_3^{(3)}\sigma_1^{(2)*}\sigma_2^{(2)*} \left. \right].
\end{aligned}$$

The  $\Lambda$ 's in the expression of  $\Gamma_4^{(4)}$  are evaluated at  $A = 1$ , and all coefficients are computed at the critical point ( $E = E_*$ ).

## REFERENCES

- Antiochos, S. K. 1979, *Ap. J. (Letters)*, **232**, L125.  
 Antiochos, S. K., Shoub, E. C., An, C. H., and Emslie, A. G. 1985, *Ap. J.*, **298**, 876.  
 Cheng, C., Doschek, G. A., and Feldman, U. 1976, *Ap. J.*, **210**, 836.  
 Chiuderi, C., Einaudi, G., and Torricelli-Ciamponi, G. 1981, *Astr. Ap.*, **97**, 27.  
 Craig, I. J. D., and McClymont, A. N. 1981, *Nature*, **294**, 333.  
 ———. 1986, *Ap. J.*, **307**, 367.  
 ———. 1987, *Ap. J.*, **318**, 421.  
 Craig, I. J. D., McClymont, A. N., and Underwood, J. H. 1978, *Astr. Ap.*, **70**, 1.  
 Craig, I. J. D., and Schulkes, R. M. S. M. 1985, *Ap. J.*, **296**, 710.  
 Doschek, G. A., et al. 1986, in *Energetic Phenomena on the Sun*, ed. M. Kundu and B. Woodgate (NASA Conf. Pub. 2439), Chap. 4.  
 Feldman, U., and Doschek, G. A. 1977, *Ap. J. (Letters)*, **216**, L119.  
 Gómez, D., Sicardi Schifino, A., and Ferro Fontán, C. 1990, *Ap. J.*, **352**, 318 (Paper I).  
 Haken, H. 1983, *Advanced Synergetics* (Berlin: Springer-Verlag).  
 Hassard, B. D., Kazarinoff, N. D., and Wan, W. H. 1981, *Theory and Applications of Hopf Bifurcation* (Cambridge: Cambridge University Press).  
 Hood, A. W., and Priest, E. R. 1980, *Astr. Ap.*, **87**, 126.  
 Iooss, G., and Joseph, D. D. 1980, *Elementary Stability and Bifurcation Theory* (Berlin: Springer-Verlag).  
 Kuin, N. P. M., and Martens, P. C. H. 1982, *Astr. Ap.*, **108**, L1.  
 Martens, P. C. H. 1984, *Phys. Rept.*, **115**, 315.  
 McClymont, A. N., and Craig, I. J. D. 1985a, *Ap. J.*, **289**, 820.  
 ———. 1985b, *Ap. J.*, **289**, 843.  
 Meunier, C., and Verga, A. 1988, *J. Stat. Phys.*, **50**, 345.  
 Pakkert, J. W., Martens, P. C. H., and Verhulst, F. 1987, *Astr. Ap.*, **179**, 285.  
 Peres, G., Rosner, R., Serio, S., and Vaiana, G. S. 1982, *Ap. J.*, **252**, 791.  
 Rosner, R., Tucker, W. H., and Vaiana, G. S. 1978, *Ap. J.*, **220**, 643.  
 Spitzer, L. 1962, *Physics of Fully Ionized Gases* (New York: Interscience).  
 Vesecky, J. F., Antiochos, S. K., and Underwood, J. H. 1979, *Ap. J.*, **233**, 987.

CONSTANTINO FERRO FONTÁN and ANIBAL SICARDI SCHIFINO: Departamento de Física, Facultad de Ciencias Exactas y Naturales—Universidad de Buenos Aires, Ciudad Universitaria, (1428) Buenos Aires, Argentina

DANIEL GÓMEZ: Instituto de Astronomía y Física del Espacio, C.C. 67—Suc. 28 (1428) Buenos Aires, Argentina